Late time evolution of unforced inviscid two-dimensional turbulence

By DAVID G. DRITSCHEL,[1] RICHARD K. SCOTT,[1] CHARLIE MACASKILL,[2] GEORG A. GOTTWALD,[2] AND CHUONG V. TRAN[1]

[1]School of Mathematics and Statistics, University of St Andrews, St Andrews KY16 9SS, UK
e-mail: dgd@mcs.st-and.ac.uk, chuong@mcs.st-and.ac.uk, rks@mcs.st-and.ac.uk

[2]School of Mathematics and Statistics, University of Sydney, NSW 2006, Australia
e-mail: charlie@maths.usyd.edu.au, gottwald@maths.usyd.edu.au

(Received 14 November 2008)

We present and analyze numerical results for the turbulent evolution of a perfectly inviscid, unforced, two-dimensional fluid. At large scales, we perform a high resolution vortex-in-cell simulation, complemented at moderate to small scales by a high-resolution CASL simulation. To analyze the results we combine a recent theory of vortex self-similarity (Dritschel *et al.* 2008), applicable to the range of scales spanned by the vortex population, with the theory of equipartition (Fox & Orszag 1973), applicable to the larger scales at late times when the rate of evolution becomes very slow. Our new model predicts an energy spectrum $\mathcal{E}(k,t) \propto t^{1/3}k^1$ at large scales, together with $\mathcal{E}(k,t) \propto t^{-2/3}k^{-5}$ over the vortex population, and finally $\mathcal{E}(k,t) \propto t^{-1}k^{-3}$ over an exponentially-widening small-scale range dominated by incoherent filamentary debris. This filamentary range moves to progressively higher wavenumbers, carrying with it nearly all of the enstrophy (mean-square vorticity) but negligible energy.

Analogous results follow for a three-dimensional (rotating stratified) quasi-geostrophic fluid. In this case, equipartition at late times gives rise to a spectrum $\mathcal{E}(k,t) \propto t^{9/20}k^2$ at large scales, while the emergence of a self-similar population of vortices gives rise to a spectrum $\mathcal{E}(k,t) \propto t^{-3/4}k^{-6}$ at intermediate scales. As in two dimensions, the small-scale spectrum has the form $\mathcal{E}(k,t) \propto t^{-1}k^{-3}$, and moves to ever higher wavenumbers while spreading exponentially.

1. Introduction

One of the most fascinating aspects of fluid flows is turbulence. Turbulence is inherently nonlinear, operating over a wide range of spatial and temporal scales (cf. Davidson, 2004 & refs.). This range grows with the Reynolds number, or the inverse of viscosity. Yet turbulence is not a state of complete disorder, but rather a semi-organised state exhibiting coherent structures (e.g. vortices) and self-similar scaling properties (e.g. power-law spectra).

Turbulence is found in a great number of physical systems, ranging in scale from quantum to astrophysical dimensions. There is little hope of a universal theory applicable to all systems, but some idealised systems now appear to be within reach. Two such systems are the focus of the present paper: the two-dimensional (2D) Euler equations, and the three-dimensional (3D) quasi-geostrophic (QG) equations, the latter governing the motion of a rapidly rotating, stably-stratified geophysical fluid. The systems are in many

ways analogous: both have a materially conserved quantity, vorticity or potential vorticity, respectively. In the inviscid situation considered here, both systems evolve purely by two-dimensional advection, which is layerwise in the case of 3D QG flow, with no vertical motion. For both cases there is an inverse energy cascade to large scales and a direct enstrophy cascade to small scales, and both are predicted to have a k^{-3} small-scale energy spectrum over scales not directly affected by viscosity (Batchelor, 1969; Charney, 1971).

It has been recognized for some time that the k^{-3} decay of the energy spectrum, found independently by Batchelor (1969) and Kraichnan (1967) in 2D turbulence, is not sufficient to explain the observed steeper spectra (see for example McWilliams, 1984). These theories are local in wave number space and do not take into account the non-local effect of vortices in transporting energy and enstrophy. Since then, several scaling theories have been proposed stressing the importance of vortices for the energy transport in spectral space. Benzi *et al.* (1988) and Benzi *et al.* (1992) linked the statistics of vortex populations to the energy spectrum. They numerically fitted an algebraically decaying vortex population with number density $n(A,t) \sim A^{-\xi}$ (where $n(A,t)\mathrm{d}A$ gives the average number of vortices with areas between A and $A + \mathrm{d}A$ over a sample area A_s in the plane) to deduce that the energy spectrum associated with the vortices decays more steeply than predicted by the Batchelor scaling (Batchelor 1969). The temporal scaling of the vortex number density was addressed in Carnevale *et al.* (1991) and Weiss & McWilliams (1993). Carnevale *et al.* (1991) assumed that, in addition to energy, the maximal vorticity during vortex interactions is conserved. Dimensional arguments then lead to an algebraic decay in time of the vortex number density $n(A,t)$. Their analysis however assumes vortices of one particular size, and does not predict the value of the scaling exponent. In Dritschel *et al.* (2008) we presented a model which unifies the spatial and temporal scaling theories. We argued that a self-similar vortex population naturally arises in two-dimensional turbulence, and that this population is characterised by a vortex number density $n(A,t) \propto t^{-2/3}A^{-1}$. We showed that this generates an energy spectrum $\mathcal{E}(k,t) \propto t^{-2/3}k^{-5}$ over the range of scales containing the vortex population. Moreover, this implies that the enstrophy in the vortex population decays like $t^{-1/3}$ through partially destructive interactions, which produce incoherent filamentary debris carrying nearly all of the enstrophy to small scales at late times. Meanwhile, and for consistency, the mean radius of the largest vortices slowly grows like $t^{1/6}$, sending energy to progressively larger scales at a diminishing rate proportional to $t^{-5/6}$. These predictions were verified by an ensemble of ultra-high resolution numerical simulations, and are consistent with previous numerical simulations (Benzi *et al.* 1992, Bracco *et al.* 2000, Clercx *et al.* 1999, Weiss & McWilliams 1993). For details, the reader is referred to Dritschel *et al.* (2008). In appendix A, we sketch an analogous model for 3D QG flow.

In the present paper, we consider scales larger than any vortex in an infinite domain in order to examine the limit $t \to \infty$ without the effects of domain boundaries or periodicity. We argue that as the flow evolution slows down at late times, the large-scale evolution approaches equipartition (Kraichnan, 1967; Fox & Orszag 1973), with energy becoming equally distributed among Fourier modes over an increasing range of scales. This tendency is illustrated in §2 through a novel point-vortex experiment starting from small-scale initial conditions. In §3, vortex self-similarity (Dritschel *et al.* 2008) and large-scale equipartition are combined in a model of the long-time turbulent decay. Using conservation of energy and enstrophy, and assuming that the smallest scales stretch exponentially fast (at a constant growth rate), this model predicts that the steep k^{-5} energy spectrum associated with the vortex population slowly spreads over the range

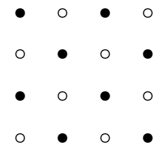

FIGURE 1. Staggered array of point vortices (• = positive, ◦ = negative) in a single grid box used as the initial conditions. The vortices are separated by $\Delta x/4$ both horizontally and vertically, where Δx is the grid size.

$m(t) \lesssim k \lesssim f(t)$, with $f(t) \sim t^{1/6}$ and $m(t) \sim t^{-1/6}$. Meanwhile, the shallower k^{-3} energy spectrum associated with incoherent filamentary debris is pushed out to ever higher wavenumbers, $k \gtrsim f(t) \sim t^{1/6}$. Support for this model is provided in §4 via a large ensemble of high resolution numerical simulations. The paper concludes in §5.

2. Large-scale dynamics

At scales much larger than any vortex, vortices appear point-like yet may collectively exhibit large-scale motions, e.g. in the form of clusters of like-signed vortices. This *self-organisation* was discussed early on in this context by Onsager (1949) and many others since. Onsager used a thermodynamical analogy to predict clustering depending on properties of the initial vortex distribution, like the proximity of like or opposite-signed vortices. Onsager considered point vortices having finite circulations but infinitesimal size, and it seems appropriate to revisit this model to understand the development of large-scale order in turbulence. Specifically, we wish to understand the form of the energy spectrum developing from an inverse cascade of energy from an initial small-scale reservoir containing disorganised or incoherent vortical motions.

To this end, we carried out a large simulation of $4096^2 \approx 17$ million vortices in a 2D doubly-periodic domain. We used the vortex-in-cell (VIC) method (cf. Christiansen & Zabusky, 1973) on a 1024^2 grid to speed up the calculation. In the VIC method, the vorticity at a grid point is obtained by a weighted sum of the vortex circulations in the surrounding 4 grid boxes, using the standard Fresnel weights associated with bi-linear interpolation. The gridded vorticity field ω so obtained is then 'inverted' via FFTs to obtain the streamfunction $\psi = \Delta^{-1}\omega$ and the velocity field $\boldsymbol{u} = \nabla^{\perp}\psi = (-\psi_y, \psi_x)$ on the grid. Finally, $\boldsymbol{u}$ is interpolated (bi-linearly) to the positions of the 17 million vortices and used to advect them forward within a 4^{th}-order Runge-Kutta time-stepping scheme.

So far this is standard. The novelty, we believe, lies in our set up of the initial conditions. To track the inverse energy cascade, we had to ensure that initially very little energy was contained in scales larger than the grid size. This is virtually impossible to achieve from a random distribution of vortices, even 17 million of them. Random placement invariably leads to a k^{-1} energy spectrum (as discussed by Davidson, 2007), spoiling any hope of observing an inverse cascade. Instead, in each of the 1024^2 grid boxes, we placed 16 vortices in a nearly regular array with 8 positive vortices (each with circulation Γ) and 8 negative vortices (each with circulation $-\Gamma$), staggered as shown in figure 1. For a perfectly regular array in each grid box, the net vorticity at each grid point is identically zero, so there is in fact no energy (or enstrophy) at and above the grid scale.

To get things going, each vortex is displaced in x and in y by a uniformly-distributed random number lying between $-0.001\Delta x$ and $+0.001\Delta x$ where Δx is the grid spacing. This generates a weak k^1 energy spectrum (see below) which is subsequently overwhelmed by the inverse cascade.

The vortex circulation Γ is chosen so that the vorticity ω would be 4π for a regular

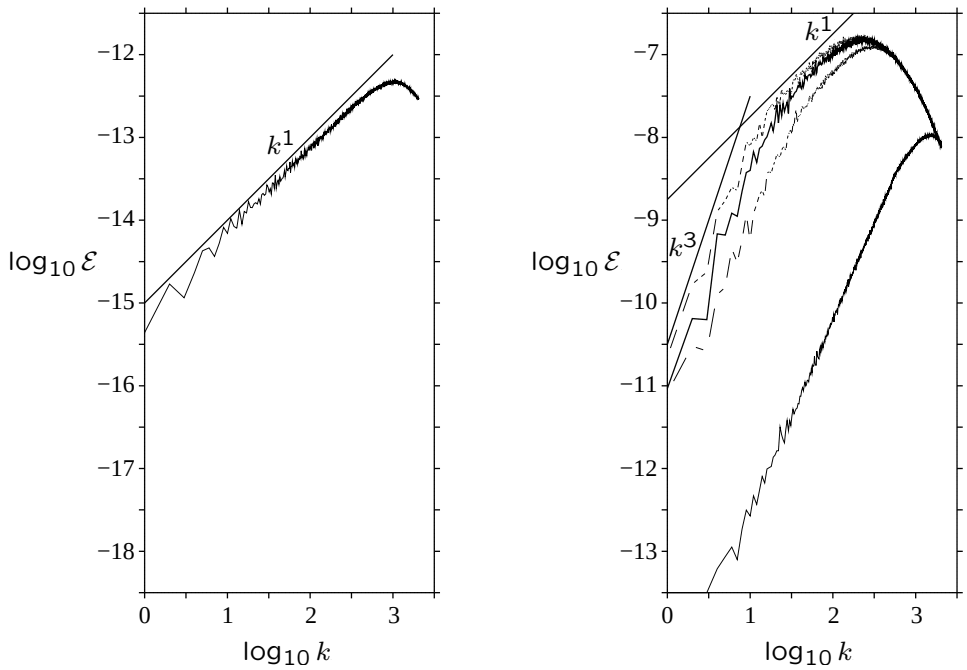

FIGURE 2. Energy spectra at $t = 0$ (left) and (right) at times $t = 100$ (thin solid line), 200 (long dashed line), 300 (bold solid line) and 400 (short dashed line).

array of positive vortices in the grid boxes surrounding a given grid point. This requires $16\Gamma = 4\pi(\Delta x)^2$. The vorticity-based time scale is then unity.

We now turn to the results of this simulation. By time $t = 100$, there is already a huge growth of energy at large scales, and the energy continues to grow (as energy cascades from sub-grid to super-grid scales) until about $t = 500$. Figure 2 shows the energy spectra $\mathcal{E}(k,t)$ at $t = 0$ (left panel), and $t = 100$, 200, 300 and 400 (right). Note there is a difference of 5 orders of magnitude in the energy ranges plotted in the two plots. From $t = 500$ onwards, the energy evolves much more slowly, and fastest at the largest scales (or lowest wavenumbers) — see figure 3 (left) for $t = 500$, 1000, 1500 and 2000, and (right) for $t = 2000$ individually. Figure 4 shows the temporal evolution of the total energy and enstrophy. One sees clearly the initial rapid increase in energy and enstrophy and the slower evolution to a plateau at later times.

The most striking feature exhibited by the energy spectra in figure 3 is their convergence to some fixed form over an increasingly wide range of wavenumbers. In time, the growth in energy becomes confined to progressively lower wavenumbers or larger scales, as can be seen in the streamfunction field ψ, shown in figure 5 at $t = 200$, 500 and 2000. The largest scale in ψ coincides with the transition from $\mathcal{E} \sim k^1$ to k^3.

A k^3 range is expected, for sufficiently small k, based on the mathematical analysis of Tran & Dritschel (2006a), who proved that $\mathcal{E}(k,t) \le Ck^3t^2$, for some constant C proportional to the square of the total energy, starting from $\mathcal{E}(k,0) = 0$ over this wavenumber range. The k^3 scaling behaviour at large scales can be related to the non-vanishing total angular momentum of the vortices through the Loitsyansky integral (see Davidson 2007). This growth in $\mathcal{E}(k,t)$ at small k is not incompatible with the widening k^1 range seen in figure 3 (and quantified below), and, for example, could be modelled by the spectral

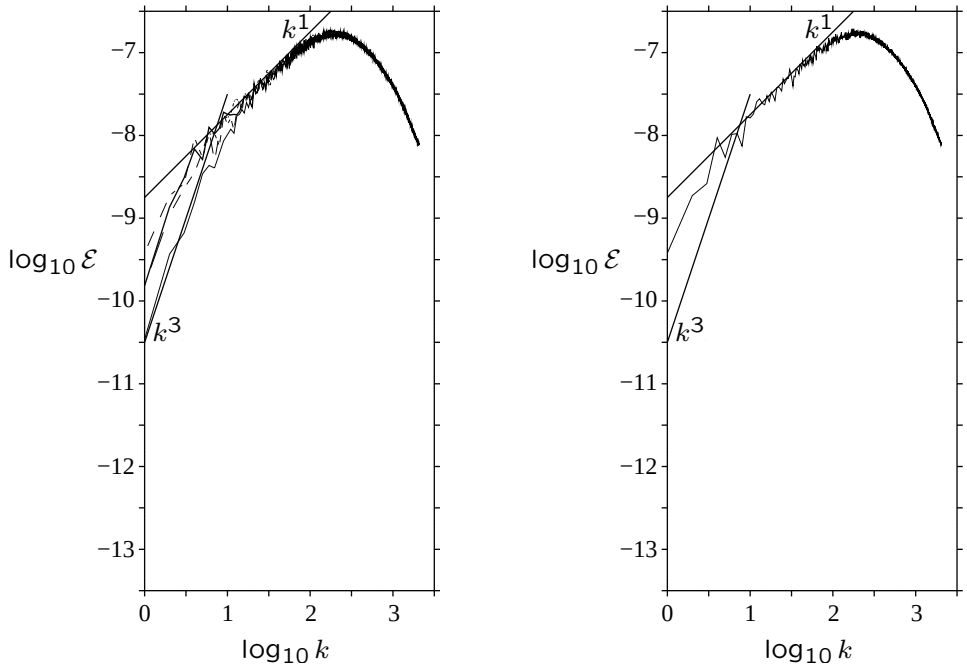

FIGURE 3. Energy spectra (left) at times $t = 500$ (thin solid line), 1000 (long dashed line), 1500 (bold solid line) and 2000 (short dashed line), and (right) at $t = 2000$ individually.

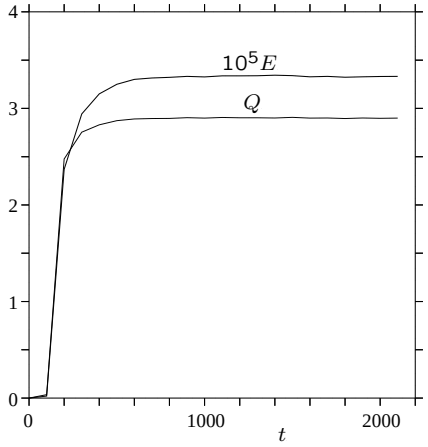

FIGURE 4. Total energy E (multiplied by 10^5) and enstrophy Q in wavenumbers $k \leq 512$ versus time t. Note that the initial growth in E and Q is approximately exponential.

form

$$\mathcal{E}(k,t) \sim \frac{a_0 k^3}{k^2 + b^2} \tag{2.1}$$

for $a_0 \approx$ constant and $b(t)$ a decreasing function of t (no faster than t^{-1} to be consistent with $\mathcal{E}(k,t) \leq Ck^3t^2$ for $k \ll b$). This spectral form however is too simple to describe the nearly fixed form of the spectrum for $k \gg b$.

That fixed form, we argue, is a consequence of *equipartition*, in which a linear combination of energy $|\hat{\boldsymbol{u}}|^2$ and enstrophy $k^2|\hat{\boldsymbol{u}}|^2$ spreads itself uniformly among the Fourier

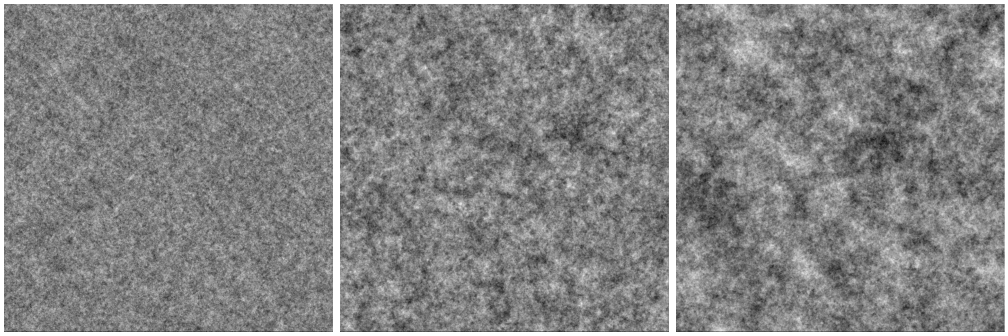

FIGURE 5. Streamfunction $\psi(\boldsymbol{x}, t)$ at $t = 200$, 500 and 2000 (left to right). A linear greyscale is used from the minimum (black) to maximum (white) values.

modes (Kraichnan, 1967). This gives rise to the equipartition spectrum

$$\mathcal{E}_{\rm eq}(k) = \frac{c_1 k}{k^2 + p^2} \tag{2.2}$$

where the constants c_1 and p are determined from the total energy $E = \int \mathcal{E}_{\rm eq} {\rm d}k$ and enstrophy $Q = \int k^2 \mathcal{E}_{\rm eq} {\rm d}k$, integrated over $0 \le k \le k_{\rm max}$, where $k_{\rm max}$ is the maximum wavenumber used in the truncated inviscid dynamical model. Fox & Orszag (1973) illustrate how the spectral shape (controlled by p^2) depends on the ratio Q/E, and discuss the approach to equipartition from non-equilibrium initial conditions. They conducted truncated spectral simulations of inviscid two-dimensional turbulence and confirmed that $\mathcal{E}(k,t) \to \mathcal{E}_{\rm eq}(k)$ at large times.

The present point vortex simulation appears to exhibit similar characteristics. It too has truncated dynamics, in the sense that no enstrophy cascade can occur below a certain scale (the individual point vortices are neither created nor destroyed). This appears to be sufficient for the flow to approach equipartition. But the definitive test is how well the spectra in figure 3 match the equipartition spectrum (2.2) for the known values of E and Q. Clearly the equilibrium energy spectrum (2.2) does not explain the energy spectrum at large scales where we observe a k^3 range. However since this range is decreasing over time and being invaded by the k^1 spectrum, we may introduce another time-dependent parameter $b(t)$ and modify (2.2) at low k to have the form of (2.1), leading to the hybrid spectrum

$$\mathcal{E}(k,t) \sim \frac{ck^3}{(k^2 + b^2)(k^2 + p^2)} \ . \tag{2.3}$$

The amplitude $c(t)$ and the two wavenumbers $b(t)$ and $p(t)$ can be determined by fitting to E, Q and the integral $S = \int k^{-2} \mathcal{E} {\rm d}k$ which is the mean-square streamfunction. The parameter $b(t)$ measures the departure from the equilibrium spectrum (2.2) and for $b(t) \to 0$ we have $\mathcal{E}(k,t) \to \mathcal{E}_{\rm eq}(k)$. Note that S is not conserved in the exact dynamics, but $k^{-2}\mathcal{E}$ peaks around the wavenumber b controlling the transition between large and intermediate scales. Figure 6 shows how well (2.3) matches the actual energy spectra over $0 \le k \le k_{\rm max} = 512$ at early, intermediate and late times in the point vortex simulation. The agreement is excellent across all wavenumbers, and uniformly in time for $t \ge 300$. Note that these results are *not* obtained by a least-squares curve fit, but merely by equating $\int k^{-2}\mathcal{E}{\rm d}k$, $\int \mathcal{E}{\rm d}k$ and $\int k^2 \mathcal{E}{\rm d}k$ for $\mathcal{E}$ in (2.3) to the known values of S, E and Q in the point vortex simulation.

The parameters b, c and p are displayed in figure 7 as a function of time for $t \ge 300$.

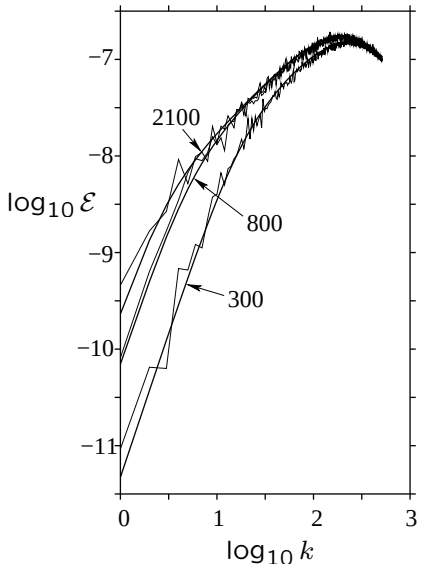

FIGURE 6. Actual energy spectra at $t = 300$, 800 and 2100 (thin lines) compared to hybrid-equipartition spectra (bold lines).

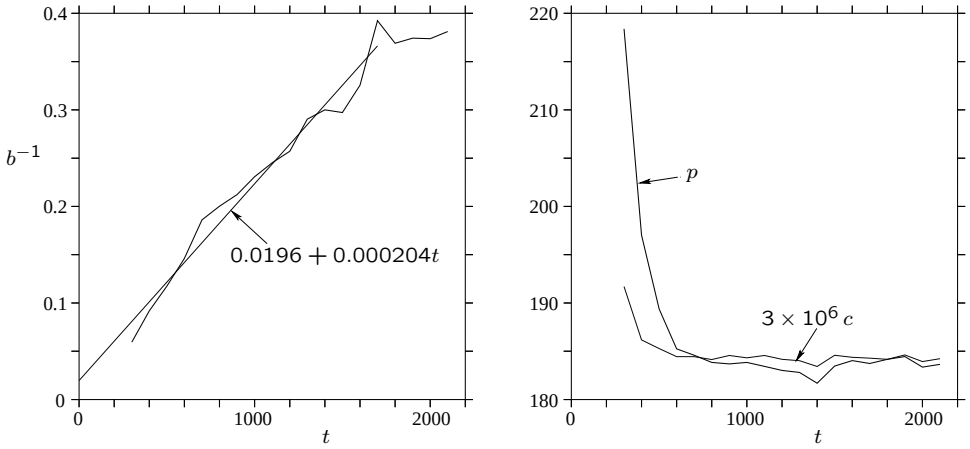

FIGURE 7. Time evolution of the inverse large-scale wavenumber b (left), spectral amplitude c (right) together with the peak wavenumber p (also right). The linear fit on the left was obtained by a least-squares analysis over $300 \leq t \leq 1700$.

Note that $c(t)$ and $p(t)$ rapidly tend to constant values, while the wavenumber $b(t)$ diminishes like t^{-1}, consistent with the bound obtained by Tran & Dritschel (2006a). For times $t > 1700$, the nearly linear increase in $1/b$ is arrested. At these times, the simulation becomes increasingly affected by the finite box size, preventing further scale growth. But we clearly can see the trend towards the equilibrium spectrum (2.2).

We now consider how equipartition relates to the physical properties of the vortex distribution. Davidson (2007) has shown that a random distribution of vortex dipoles gives rise to a k^1 energy spectrum at scales larger than the dipoles. This suggests that our simulation is dominated by dipoles at scales comparable to the energy-enstrophy scale L (where the spectrum changes over from k^{-1} to k^1 around $k = p$). Figure 8 shows that this is indeed the case, each dipole being composed of many point vortices. Note

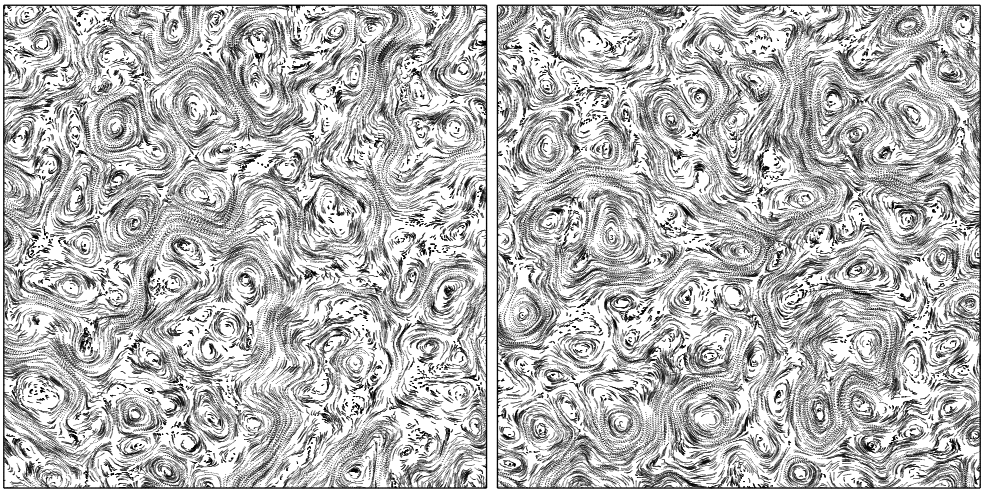

FIGURE 8. Point-vortex trajectories over a single unit of time at (left) $t = 800$ and (right) $t = 2000$. Only a thousandth ($1/32^2$) of the domain is shown. The energy-enstrophy scale L in each case is shown beneath each plot. Note that the characteristic large scale $2\pi/b \sim 100L$.

that the scale of the dipoles does not grow appreciably over time, but remains of order L. Moreover, the dipoles are space filling, and an examination of their time evolution shows that they are short lived (with life times comparable to the enstrophy timescale $1/Q^{1/2}$).

As shown next, a random distribution of dipoles implies that the ensemble mean vorticity $\langle|\omega|\rangle$ over an area of size A should scale as $A^{-3/4}$. The statistical proof is as follows. In any sufficiently large area A, the expected number of dipoles is proportional to A. Within A, the dipoles contribute nothing to the mean vorticity, but on the periphery of A, some halves of dipoles will be in A and others will not. Hence, there will be a surplus of positive or negative vortices. The mean number of randomly distributed surplus vortices scales as the square-root of the number of dipoles on the periphery of A (since the orientation of the dipoles is uniformly distributed). But the number of dipoles on the periphery is proportional to the perimeter of A, which is itself proportional to $A^{1/2}$. Hence, the mean number of surplus vortices scales like $A^{1/4}$. This divided by the area A is proportional to the mean vorticity over A, and therefore $\langle|\omega|\rangle \propto A^{-3/4}$. Figure 9 shows just how good this prediction is, over a very wide range of areas A extending from the grid scale to the domain scale. Note that a random distribution of vortex monopoles, by similar arguments, would give $\langle|\omega|\rangle \propto A^{-1/2}$. A reduction in slope toward $-1/2$ is just visible in figure 9 at scales smaller than the energy-enstrophy scale L. As can be seen from figure 8, these scales are below the scale of the dipoles and are characterised by individual monopoles (the point vortices themselves).

3. Late time evolution at all scales

The main limitation of the point vortex model just described is that the individual vortices cannot merge and exhibit an enstrophy cascade (p is constant in (2.2)). This cascade transfers coherent enstrophy contained within the vortices to filaments, and additionally results in a slow $t^{1/6}$ growth of large-scale vortices (Dritschel *et al.* 2008). The observed tendency toward equipartition exhibited by the point vortices, however, is a direct result of their stationary population characteristics. Nevertheless, we argue that

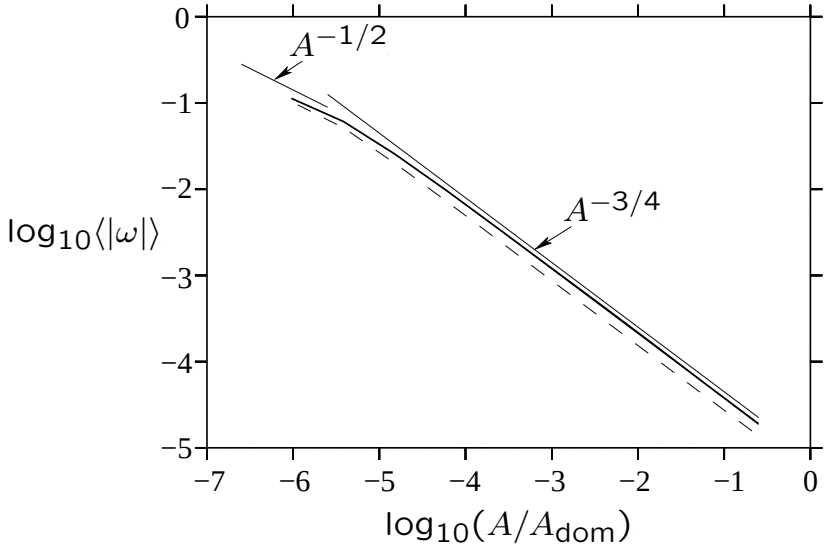

FIGURE 9. Ensemble mean vorticity $\langle|\omega|\rangle$ versus the sampling area A in the point vortex simulation at times $t = 200$ (short-dashed line) and 600 (bold). We note that at time $t = 2000$ the curve is indistinguishable from that at $t = 600$. Lines proportional to $A^{-3/4}$ and $A^{-1/2}$ are shown for reference. Note that $L^2/A_{\mathrm{dom}} \approx 10^{-5}$ at the latter two times.

evolving two-dimensional turbulence will form an equipartition spectrum at large scales, precisely because the evolution is so slow and becomes ever slower in time. Eventually, there is time for equipartition to become established at all but the very largest scales, which must remain bounded by a steeper k^3 spectrum (Tran & Dritschel, 2006a).

To analyze the numerical results at the large scales we propose here a simple spectral form incorporating three basic elements:

(1) large-scale equipartition over a range $k \lesssim m(t)$,

(2) a self-similar vortex population over a range $m(t) \lesssim k \lesssim f(t)$, and

(3) a filamentary cascade over a range $f(t) \lesssim k \lesssim d(t)$.

A spectral form with these properties is

$$\mathcal{E}(k,t) = \frac{ck(1 + k^2/f^2)}{(k^2 + m^2)^3}\,. \tag{3.1}$$

We stress that this spectrum is chosen simply to deduce the spectral transition wavenumbers m and f. It is not a mathematical model like the equipartion spectrum (2.2) proposed by Fox & Orszag (1973). Here $m(t)$ is a wavenumber associated with the maximum vortex size (m can be defined by the coherent energy-enstrophy centroid, $m \approx \sqrt{Q_{\mathrm{coh}}/E_{\mathrm{coh}}}$, obtained by integrating the spectrum over the vortex wavenumbers $m(t) \lesssim k \lesssim f(t)$). The wavenumber $f(t)$ marks the transition scale from vortices to filaments, and $d(t)$ is the leading edge of the 'enstrophy front', assumed to be increasing exponentially (see below). The final coefficient $c(t)$ is proportional to the vortex density (Dritschel *et al.* 2008). Notice for simplicity we ignore the steep k^3 range at $k \ll m$; this range contributes negligibly to both the energy and the enstrophy. Moreover, we do not incorporate the k^{-1} range of the equipartition spectrum (2.2). This is because the transition from k^1 to k^{-1} in (2.2) occurs at the energy-enstrophy centroid $p \approx \sqrt{Q/E}$, which is much larger than its coherent counterpart $m \approx \sqrt{Q_{\mathrm{coh}}/E_{\mathrm{coh}}}$, since $Q_{\mathrm{coh}} \ll Q$ at late times (while $E_{\mathrm{coh}} \approx E$).

At sufficiently late times (i.e. many eddy turnaround times based on r.m.s. vorticity), vortex self-similarity predicts $c(t) \sim t^{-2/3}$ and $m(t) \sim t^{-1/6}$ (Dritschel *et al.* 2008). However, the 'filament transition' wavenumber $f(t)$ is not predicted. Instead here we determine $f(t)$ from conservation of energy E and enstrophy Q, together with an assumption on the growth of the 'enstrophy front' at $k = d(t)$. We argue that the thinnest filaments, at the scale $L_d \propto d^{-1}$, are essentially passive and thus likely thin exponentially fast, i.e. $d(t) \sim e^{\gamma t}$ where γ is the mean strain rate associated with larger scales. It is conceivable that γ scales with the r.m.s. vorticity contained within the larger scales, but it seems more plausible that γ scales with the characteristic vorticity magnitude ω_v within the vortices, which efficiently capture and twist filamentary debris as they criss-cross space. ω_v varies little across the vortex population (Dritschel *et al.* 2008) and is time invariant. The r.m.s. vorticity on the other hand decreases like $t^{-1/6}$ due to the decreasing area fraction covered by the vortices (Dritschel *et al.* 2008). Since there is little practical difference, we choose the simpler assumption that γ is constant.

This assumption is well supported by simulation results for Navier-Stokes turbulence (Dritschel *et al.* 2007), where it was shown that the palinstrophy P (or mean-square vorticity gradient) reaches a maximum at a time $t = t_p \approx c_0 + c_1 \ln \mathrm{Re}$ where Re is the Reynolds number. Thereafter, P decreases by viscous dissipation. But the time t_p measures the time it takes the enstrophy front to reach the scale of viscous dissipation ℓ_{diss}. But $\mathrm{Re} \propto \ell_{\mathrm{diss}}^{-2}$, and hence $\ell_{\mathrm{diss}} \sim e^{-\gamma t_p}$ for some constant γ. Identifying ℓ_{diss} with $1/d$ in the inviscid context, and t_p with t, we arrive again at $d(t) \sim e^{\gamma t}$.

We now determine the scaling of the filament transition wavenumber $f(t)$. Without loss of generality, we are free to nondimensionalise length and time by taking $E = Q = 1/2$. Using then (3.1), elementary integration yields

$$\frac{4}{c}\int_0^d \mathcal{E}(k,t)\mathrm{d}k = \frac{2}{c} = \frac{1}{m^4} + \frac{1}{f^2 m^2} + \mathcal{O}\left(\frac{1}{f^2 d^2}\right) \tag{3.2}$$

$$\frac{4}{c}\int_0^d k^2 \mathcal{E}(k,t)\mathrm{d}k = \frac{2}{c} = \frac{1}{m^2} + \frac{4\log(d/m) - 3}{f^2} + \mathcal{O}\left(\frac{1}{d^2}\right). \tag{3.3}$$

At late times $t \gg 1$, the wavenumbers become increasingly well separated, $m \ll f \ll d$, and moreover $\log(d/m) \sim t \gg 1$. Retaining therefore only the dominant terms, we have $c \approx 2m^4$ from energy conservation (which is consistent with $c \sim t^{-2/3}$ and $m \sim t^{-1/6}$) and

$$\frac{1}{m^4} \approx \frac{1}{m^2} + \frac{4\log(d/m)}{f^2} \tag{3.4}$$

from enstrophy conservation, which implies

$$f \approx 2m^2 \frac{\sqrt{\log(d/m)}}{\sqrt{1-m^2}}\,. \tag{3.5}$$

At late times, $m \ll 1$. Now we use our assumption that the enstrophy front increases exponentially $d(t) \sim e^{\gamma t}$ to obtain the following scaling for the filament transition wavenumber:

$$f \sim t^{1/6}\,. \tag{3.6}$$

A postiori, this justifies $m \ll f \ll d$.

This simple model predicts energy growth $\mathcal{E}(k,t) \propto t^{1/3}k^1$ in the equipartition range at large scales $k \ll t^{-1/6}$, energy decay $\mathcal{E}(k,t) \propto t^{-2/3}k^{-5}$ over the vortex population at intermediate scales $t^{-1/6} \ll k \ll t^{1/6}$, and also energy decay $\mathcal{E}(k,t) \propto t^{-1}k^{-3}$ over the

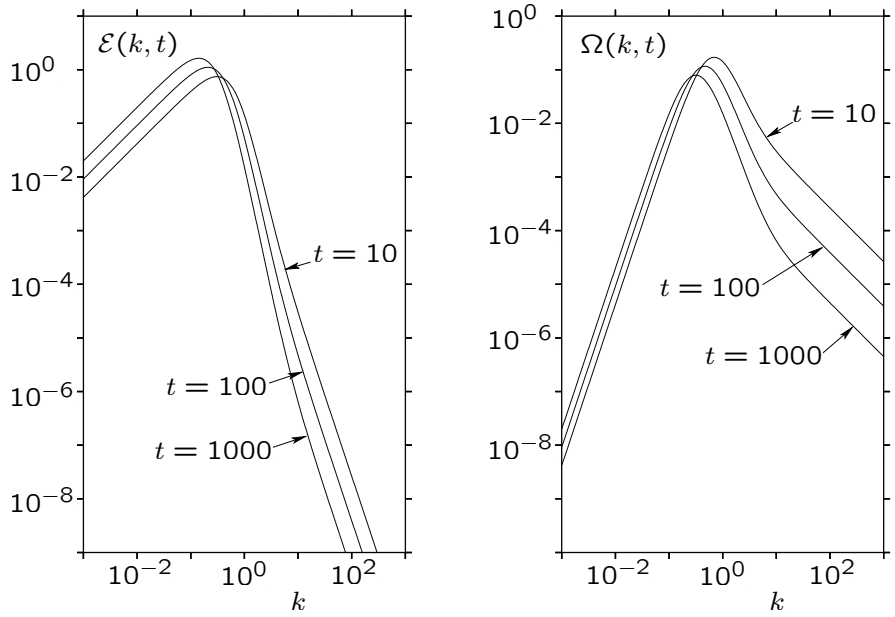

FIGURE 10. Model energy $\mathcal{E}$ and enstrophy Ω spectra (left and right) for the non-dimensional times $t = 10$, 100 and 1000 as labelled. Here, the total energy and enstrophy are both equal to 1/2. Only the range $10^{-3} \le k \le 10^3$ is shown. Logarithmic scales are used.

filamentary range at small scales $k \gg t^{1/6}$. The k^{-3} spectrum is the same as that obtained by Batchelor (1969), but in our model this spectrum applies only at high wavenumbers where filaments dominate. Moreover, this spectral tail decays more slowly than predicted by Batchelor. The t^{-1} decay is due to the exponential stretching of filaments assumed in our model. The spectral tail contains negligible energy and nearly all of the enstrophy.

The spectral evolution for this idealised model is illustrated in Figure 10, using $m = t^{-1/6}$, $d = e^t$, along with (3.2) for c and (3.5) for f. The most striking feature of this evolution is just how slow it is — there is only a small change from $t = 10$ to $t = 1000$. Notice also that the enstrophy at a fixed wavenumber to the left of the peak *increases* for a while before eventually decaying (after the peak sweeps past); nevertheless most of the enstrophy quickly ends up in the rapidly expanding tail between $k = f$ and $k = d$.

4. Comparison with numerical simulations

Support for this simple model is presented next. We carried out 20 high-resolution numerical simulations using the CASL algorithm (Dritschel & Ambaum (1997)), an efficient hybrid contour dynamics/spectral method capable of modelling a wide range of spatial scales with minimal numerical dissipation (see Appendix B). We started each simulation with the energy spectrum $\mathcal{E}(k,0) = \alpha k^3 \exp(-2k^2/k_0^2)$, with $k_0 = 32$ and α chosen so that $E = 1/2$. Then $Q(0) = k_0^2/2$. Each simulation differed only in a random number seed determining the phases of the Fourier coefficients.

The flow evolution was computed for 160 'eddy rotation periods' $T_{\rm eddy} \equiv 4\pi/\omega_{\rm rms}(0)$, where $\omega_{\rm rms}(0) = \sqrt{2Q(0)} = k_0$ is the initial r.m.s. vorticity (the peak vorticity is 4 to 5 times larger). Below, time t is in units of $T_{\rm eddy}$.

This ensemble of simulations was used previously in Dritschel *et al.* (2008) to corroborate our self-similar evolution model of the vortex population. In particular, the

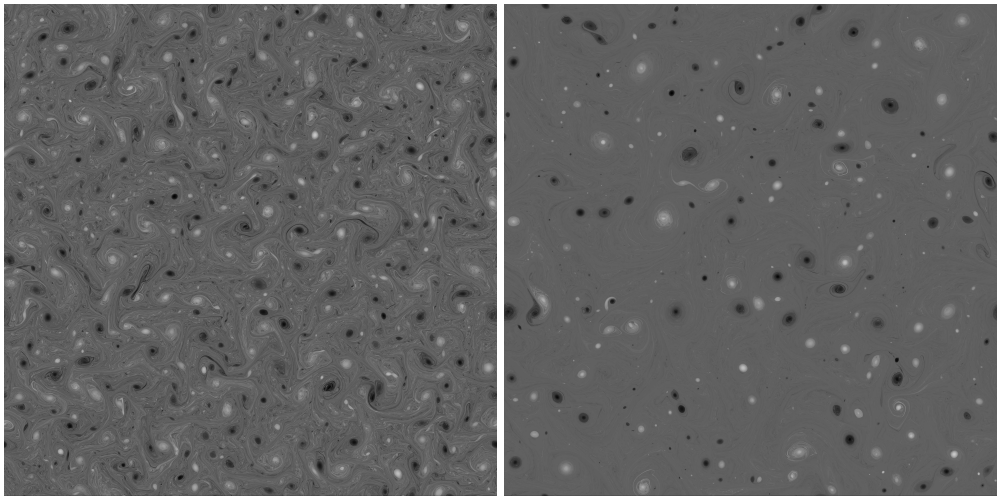

FIGURE 11. Vorticity $\omega(\boldsymbol{x}, t)$ at $t = 6$ (left) and $t = 24$ (right) in one representative simulation. A linear greyscale is used from the minimum (black) to maximum (white) values.

numerical results strongly support the development of a universal vortex number density $n(A, t) \propto t^{-2/3} A^{-1}$ (corresponding to the energy spectrum $\mathcal{E}(k, t) \propto t^{-2/3} k^{-5}$ over the range of scales containing the vortex population), and a decay of vortex enstrophy and vortex area fraction proportional to $t^{-1/3}$ over the last 90% of the evolution.

Two snapshots of the vorticity field from one simulation are shown in Figure 11. Note the prevalence of filamentary structures at early times and of vortices at later times. The flow is dominated by vortices at all but the earliest times. Figure 12 shows the enstrophy spectrum at early, intermediate and late times. Each spectrum is multiplied by $t^{2/3}$ so that, in theory, the intermediate 'vortex wavenumber range' remains steady. This appears to work well. At low wavenumbers, we observe a k^3 spectrum (which eventually saturates when energy reaches the domain scale), while at small scales we see a slowly retreating k^{-1} range. The apparently slow decay of the k^{-1} range of the enstrophy spectrum at large wavenumbers when compared to Figure 10 is due to the $t^{2/3}$ scaling we have applied.

We now quantify this spectral evolution, and compare it to the ideal evolution proposed in §3. To this end, we computed the total 'resolved' energy, enstrophy and palinstrophy (E_r, Q_r and P_r) over the wavenumbers $0 < k \leq k_r$ (with $k_r = 512$ or 2048 to check sensitivity). Here, the palinstrophy is given by $\int_0^{k_r} k^4 \mathcal{E} \mathrm{d}k$, and is equal to the mean-square vorticity gradient (divided by 2). P_r is not conserved in the inviscid limit, but it is used here to help determine the spectral parameters c, m and f in the idealised spectrum (3.1), for which

$$E_r = \frac{c}{4m^4} + \frac{c}{4f^2 m^2} \tag{4.1}$$

$$Q_r = \frac{c}{4m^2} + \frac{c}{f^2}\left[\log(k_r/m) - \frac{3}{4}\right] \tag{4.2}$$

$$P_r = \frac{c k_r^2}{2f^2} \tag{4.3}$$

approximately (for $k_r \gg f$).

The spectral parameters were determined from each simulation from early times $t = 10$ to the final time $t = 160$. They were then ensemble averaged at each time. The resulting

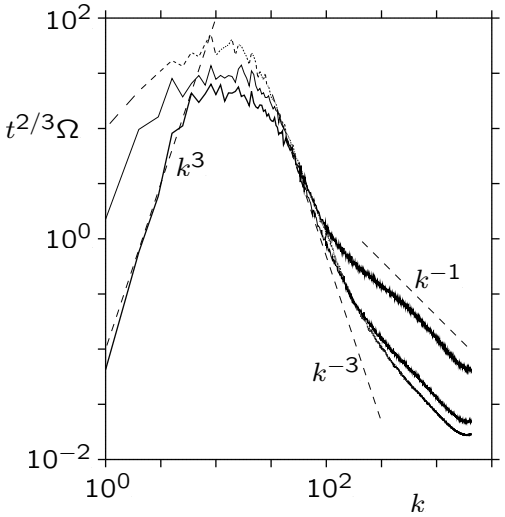

FIGURE 12. Ensemble-averaged scaled enstrophy spectra $t^{2/3}\Omega(k,t)$ at $t = 10$ (bold solid line), 40 (thin solid line) and 160 (dashed line). The temporal scaling is intended to collapse the spectra over the range of scales occupied by vortices, $m \lesssim k \lesssim f$. Various slopes are indicated.

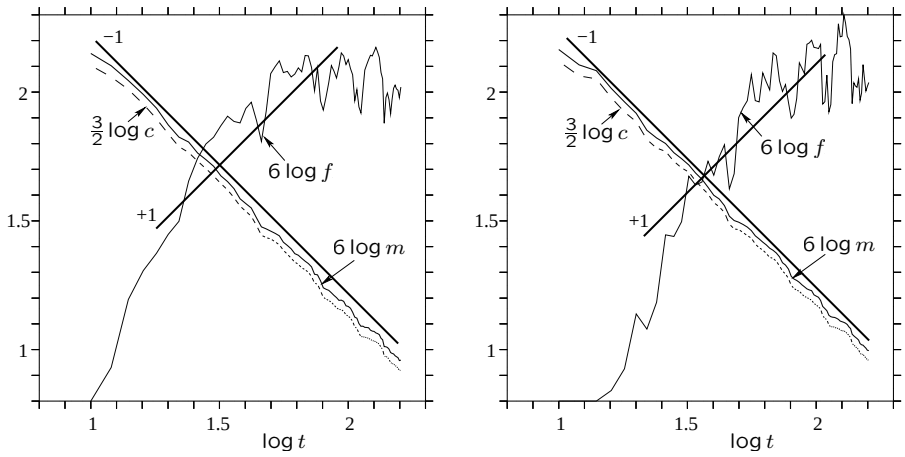

FIGURE 13. Ensemble-averaged spectral parameters $m(t)$ (bold), $f(t)$ (thin) and $c(t)$ (dashed) for two truncation wavenumbers $k_r = 512$ (left) and $k_r = 2048$ (right). Note the logarithmic scales. The units on the abscissa are arbitrary (the unscaled parameters are shown in Figure 14). Reference slopes of ± 1 are shown by the thick bold lines.

ensemble-averaged values of $m(t)$, $f(t)$ and $c(t)$ are shown in Figure 13 (log scaled) using the truncation wavenumbers $k_r = 512$ on the left and $k_r = 2048$ on the right. Figure 14 shows the corresponding unscaled results for $k_r = 2048$, emphasising the slow evolution of the wavenumbers m and f. The 'vortex wavenumber' m and the 'vortex density' c are both insensitive to the choice of k_r. Using a least-squares fit of the log-scaled data, we obtain $m \sim t^{-0.1702}$, $c \sim t^{-0.6822}$ for $k_r = 512$ and $m \sim t^{-0.1676}$, $c \sim t^{-0.6715}$ for $k_r = 2048$. These compare exceptionally well with the theoretical predictions $m \sim t^{-1/6}$ and $c \sim t^{-2/3}$ (Dritschel *et al.* (2008)).

The results for f are much less robust, with $f \sim t^{0.1188}$ for $k_r = 512$ and $f \sim t^{0.2105}$ for $k_r = 2048$. We argued for $f \sim t^{1/6}$ in §3 above. The discrepancy at early times occurs

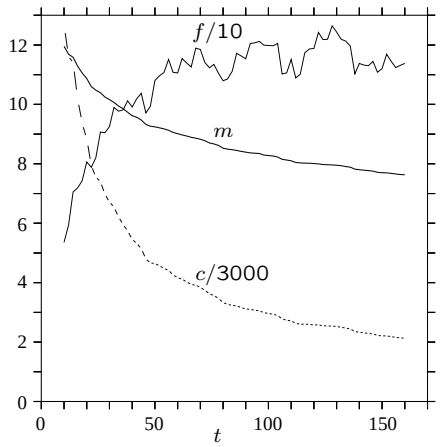

FIGURE 14. Ensemble-averaged spectral parameters $m(t)$ (bold), $f(t)$ (thin) and $c(t)$ (dashed) for $k_r = 2048$. Here the scales are linear.

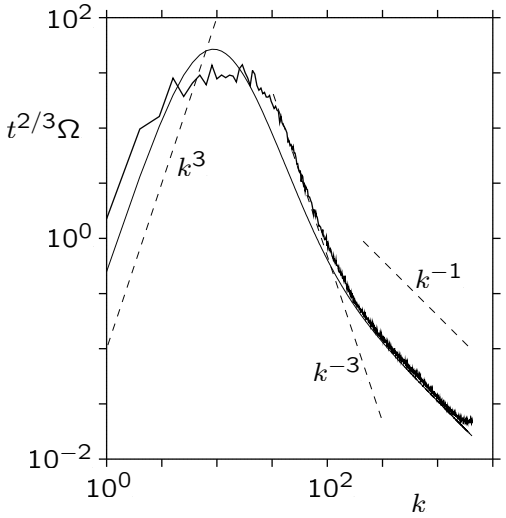

FIGURE 15. Ensemble-averaged scaled enstrophy spectra $t^{2/3}\Omega(k,t)$ at $t = 40$ (bold solid line) compared with the ideal scaled spectrum using (3.1). Various slopes are indicated.

because the spectrum has not yet filled out to k_r. Note from (4.3), f is determined only by P_r; at late times, numerical inaccuracies make P_r uncertain, particularly as P_r is dominated by the rapidly fluctuating high-k end of the spectrum. Despite the uncertainty, the numerical data are not inconsistent with our model prediction.

Finally, a comparison of the numerical and ideal model enstrophy spectra at an intermediate time of $t = 40$ is presented in Figure 15. Again c, m and f are not fit but determined from E_r, Q_r, and P_r. The ideal spectrum is more peaked but captures the spectral transitions around $k = m$ and $k = f$, and closely matches the k^{-1} tail. Importantly, the spectral parameters are *not* sensitive to the form of the ideal spectrum we have chosen, as has been verified using the 'stick' spectrum $\Omega = c\,m^{-6}k^3$ joined to ck^{-3} joined to $cf^{-2}k^{-1}$. We do not claim (3.1) is correct everywhere. What appears robust is an energy spectrum containing k^1, k^{-5} and k^{-3} ranges, with transition wavenumbers evolving according to the time-dependencies discussed. To determine the exact form

of the spectrum will require further theoretical insight, such as an improvement of the vortex self-similarity hypothesis near the maximum vortex size.

5. Concluding remarks

We have developed a new model for the late-time evolution of inviscid, unforced two-dimensional turbulence, and its three-dimensional quasi-geostrophic counterpart (in Appendix A). The model builds upon vortex self-similarity over a slowly-expanding intermediate range of scales (Dritschel *et al.* 2008). Here, we propose that the scales larger than any vortex approach a state of equipartition (Kraichnan, 1967; Fox & Orszag 1973), with energy spread uniformly among Fourier modes (except at ultra-large scales, where the energy spectrum is bounded by a constant times t^2k^3, see Tran & Dritschel, 2006a). Whereas ideal equipartition is a statistically-steady state, in our model we argue that the energy spectrum at large scales slowly grows like $\mathcal{E}(k,t) \propto t^{1/3}k^1$, and slowly cascades to ever larger scales, $k \lesssim m(t) \propto t^{-1/6}$. In particular, the flux of energy to large scales diminishes like $t^{-5/6}$. The inverse cascade becomes ever slower.

At small scales, we propose that Batchelor's k^{-3} spectrum is gradually replaced at its upper end around $k = f(t) \propto t^{1/6}$ by the steeper spectrum $\mathcal{E}(k,t) \propto t^{-2/3}k^{-5}$ associated with a self-similar population of vortices (Dritschel *et al.* 2008). The k^{-3} spectrum, we argue, spreads to high k exponentially fast, implying that the spectrum decays like t^{-1} there. This decay is slower than predicted by Batchelor (1969) by simple scale analysis. Furthermore, he did not recognise the possibility that a steeper spectrum would develop and replace the k^{-3} spectrum at intermediate scales.

We have examined our model's predictions using a large ensemble of high-resolution simulations of two-dimensional turbulence. These simulations strongly support the $t^{1/6}$ growth of the 'vortex wavenumber' m (inversely proportional to the size of the largest vortex), and the $t^{-2/3}$ decay of the 'vortex density' c. Less secure is our prediction that the 'filament transition wavenumber' f (where the energy spectrum shallows from k^{-5} to k^{-3}) grows like $t^{1/6}$. This wavenumber is sensitive to numerical inaccuracies and to spectral fluctuations at high k. Nevertheless, our results are not inconsistent with $f(t) \propto t^{1/6}$. Yet higher resolution numerical simulations are required to verify this prediction. And, further theoretical insight is needed to determine if there is a universal form of the energy spectrum.

Appendix A. Inviscid 3D quasi-geostrophic turbulence

In this appendix, we describe an analogous inviscid turbulence model for the 3D quasi-geostrophic (QG) equations. We cannot yet provide numerical support for this model due to prohibitive computational costs.

The QG equations describe the 'layerwise-2D' motion of a rapidly-rotating and stably-stratified fluid (cf. Gill 1982). In the ideal QG system considered here, the 'potential vorticity' q is transported conservatively following a layerwise incompressible flow field $u = -\partial\psi/\partial y$, $v = \partial\psi/\partial x$, $w = 0$, in precisely the same manner as the vorticity ω in the 2D Euler equations. Moreover, the two systems have the same vorticity–streamfunction relations, $q = \Delta\psi$ in 3D QG and $\omega = \Delta\psi$ in 2D — only the dimension of Laplace's operator Δ differs. In the QG equations, the vertical coordinate is stretched by the ratio of the buoyancy N_0 and Coriolis f_0 frequencies, both taken to be constant here. Finally, to complete the analogy, the total energy and enstrophy per unit volume, $\langle|\nabla\psi|^2\rangle/2$ and $\langle q^2\rangle/2$, have the same form as in 2D upon replacing q by ω.

A.1. *Vortex self-similarity*

The derivation of a self-similar vortex population closely parallels that for the 2D case presented in Dritschel *et al.* (2008). We begin by writing the enstrophy per unit volume as

$$Q = \int_0^\infty \Omega(k)\, dk = \int_0^\infty k^2 \mathcal{E}(k)\, dk \,, \tag{A 1}$$

where $\Omega(k)$ and $\mathcal{E}(k)$ are the enstrophy and energy spectra at wavenumber k. Now consider a population of vortices with a vortex number density $n(V)$; the number of vortices having volumes between V and $V + \mathrm{d}V$ is $n(V)\mathrm{d}V$ in an arbitrary domain size V_s. (Here, we are considering ensemble averages over all domains of size V_s tiling infinite space.) The part of Q associated with the vortices is

$$Q_v = \frac{1}{2V_s} \int_0^{V_s} q_v^2 V n(V)\, \mathrm{d}V \,, \tag{A 2}$$

where q_v is the potential vorticity magnitude. We now assume that most of the energy is contained within the vortices, and that q_v does not vary significantly for vortices with different volumes V. Identifying $V \sim k^{-3}$ so that $\mathrm{d}V \sim k^{-4}\, dk$, comparison of (A 1) and (A 2) gives the energy spectrum

$$\mathcal{E}(k) \sim q_v^2 V_s^{-1} n(V) k^{-9} \,. \tag{A 3}$$

For a wide-ranging population of vortices, the lack of any intrinsic scale motivates taking a powerlaw form for the vortex number density, $n(V) \sim V^{-\xi}$. Using this in (A 3), it implies $\mathcal{E} \sim k^{-9+3\xi}$. Note that the classical k^{-3} Charney (1971) spectrum is recovered for $\xi = 2$. We show next, however, that only $n(V) \sim V^{-1}$ allows for a self-similar vortex distribution. The energy spectrum then scales as

$$\mathcal{E}(k) \sim k^{-6} \,. \tag{A 4}$$

To examine scale-invariance, we first define the (ensemble-mean) volume fraction of an arbitrary volume V_s occupied by vortices

$$f_v = \frac{1}{V_s} \int_0^{V_{\max}} V n(V)\, \mathrm{d}V \,.$$

Here $V_{\max}$ is the maximal vortex size in V_s. Each vortex with volume V occupies a *zone* the volume of which is V/f_v. The sum of all zones is equal to the total volume V_s. Consider a subdomain $V_0 < V_{\max}$ which is populated by non-overlapping vortices with volumes $V \le V_0$. Arguably, these vortices typically populate a volume $V_{\rm rem}$ which is not already occupied by zones of vortices with volume $V > V_0$ since strong shear surrounding these vortices would tear apart smaller vortices. This left-over volume is just

$$V_{\rm rem} = \frac{1}{f_v} \int_0^{V_0} V n(V)\, \mathrm{d}V \,.$$

Self-similarity means that the ratio $V_0/V_{\rm rem}$ must be independent of the subdomain V_0. The only choice for $n(V)$ with this property is

$$n(V) = \frac{c}{V} \,. \tag{A 5}$$

Note that for such a density the number of vortices between μV_0 and V_0, $\mu \ll 1$, is

$$N_v = \int_{\mu V_0}^{V_0} \frac{c}{V} \mathrm{d}V = c \ln \mu^{-1} \,, \tag{A 6}$$

which is independent of the subdomain V_0, again illustrating the self-similarity associated with the special form of the vortex number density (A 5).

We now turn to the evolution of the number density $n(V,t) = c(t)/V$. Let $a(t) \sim V_{\max}^{1/3}$ denote the maximum vortex radius. The energy scales as

$$E = \frac{1}{2}\langle|\nabla\psi|^2\rangle \sim \frac{1}{2V_s}\int_0^{V_{\max}} (q_v V^{1/3})^2 V n(V)\,\mathrm{d}V \sim c a^5$$

where we have estimated $|\nabla\psi| \sim q_v V^{1/3}$, and have again assumed that q_v does not vary significantly with the vortex volume V. Conservation of energy then implies $c \sim a^{-5}$. The scaling of the enstrophy and the volume fraction can then be obtained as

$$Q_v(t) \sim a^{-2} \qquad \text{and} \qquad f_v(t) \sim a^{-2}\,. \tag{A 7}$$

The temporal behaviour of the maximal vortex radius $a(t)$ is determined by the rate of enstrophy transfer from vortices to filaments dQ_v/dt. This transfer occurs through destructive vortex interactions, most probably involving three vortices, e.g. two vortices brought together by a third, as in two-dimensional turbulence (Dritschel & Zabusky (1996)). The simplest model of this is the interaction of a vortex dipole with a third, isolated vortex. This interaction can be destructive and results in the transfer of enstrophy from the vortex population to small-scale filaments. Self-similarity now implies that the enstrophy at any scale, $q_v^2 V n(V)\mathrm{d}V$, decays at a rate which is independent of scale. We therefore equate

$$\frac{dQ_v}{dt} \sim -p_{\mathrm{col}}\frac{Q_v}{T_{\mathrm{int}}}\,, \tag{A 8}$$

where p_{col} is the collision probability of a dipole with smaller vortices and T_{int} is the time for a dipole to travel a characteristic inter-vortex distance $r(t)$. Since the collision probability is proportional to the vortex number density we have $p_{\mathrm{col}} \sim c \sim a^{-5}$. Using (A 6) the characteristic inter-vortex distance $r(t)$ of vortices with sizes between μV_0 and V_0 is given by

$$r \sim (V_0/N_v)^{1/3} \sim (V_0/c)^{1/3} \sim V_0^{1/3} a^{5/3}\,. \tag{A 9}$$

The typical time T_{int}, which measures the time a dipole of volume V_0 and width proportional to $V_0^{1/3}$ travels a distance r, can be estimated as

$$T_{\mathrm{int}} = \frac{r}{U_{\mathrm{dip}}}\,, \quad \text{with} \quad U_{\mathrm{dip}} = \frac{q_v V_0}{V_0^{2/3}} \sim V_0^{1/3} \tag{A 10}$$

being a characteristic dipole velocity. Note this implies $T_{\mathrm{int}} \sim a^{5/3}$, independent of V_0 as required by self-similarity. Substituting (A 9)–(A 10) into (A 8) we obtain a differential equation for the size of the largest vortices

$$\frac{1}{a^3}\frac{da}{dt} \sim \frac{1}{a^{26/3}} \quad \text{which implies} \quad a(t) \sim t^{3/20}\,. \tag{A 11}$$

Together with (A 5) this uniquely determines the vortex number density

$$n(V,t) \sim \frac{t^{-3/4}}{V}\,. \tag{A 12}$$

Furthermore via (A 7) we can determine the temporal scaling behaviour of the enstrophy $Q_v(t)$ and the volume fraction $f_v(t)$ as

$$Q_v(t) \sim t^{-3/10} \qquad \text{and} \qquad f_v(t) \sim t^{-3/10}\,. \tag{A 13}$$

Notably, this is a slightly slower decay than found in two dimensions.

A.2. *Large-scale dynamics and equipartition*

There is every reason to expect the 3D QG case to be similar to the 2D case, since both systems have a materially-conserved quantity, two quadratic invariants (energy and enstrophy), an inverse energy cascade, and a direct enstrophy cascade (Charney, 1971). Following Kraichnan (1967), equipartition arises when a linear combination of (total) energy $|\hat{q}|^2/k^2$ and (potential) enstrophy $|\hat{q}|^2$ spreads itself uniformly among the Fourier modes. Equipartition would then result in a spectrum of the form

$$\mathcal{E}_{\rm eq}(k) = \frac{c_1 k^2}{k^2 + p^2} \tag{A 14}$$

with the extra factor of k due to integrating over spherical shells in wavenumber space, instead of cylindrical shells in the 2D case, cf. (2.2). The parameters c_1 and p are determined from the specific values of energy E and enstrophy Q, just as in the 2D case.

A.3. *Late time spectral evolution at all scales*

At times much larger than $Q^{-1/2}$, we propose that the energy spectrum exhibits large-scale equipartition over a range $k \lesssim m(t)$, a self-similar vortex population over a range $m(t) \lesssim k \lesssim f(t)$, and a filamentary cascade over a range $f(t) \lesssim k \lesssim d(t)$. A spectrum with these characteristics is

$$\mathcal{E}(k,t) = \frac{c k^2 (1 + k^3/f^3)}{(k^2 + m^2)^4}\,. \tag{A 15}$$

(we do not claim this is the universal form, other forms give the same evolution of the spectral parameters). Here $m(t) \sim a^{-1}$ is the the wavenumber associated with the maximum vortex size (m is proportional to the coherent energy-enstrophy centroid, $\sqrt{Q_{\rm coh}/E_{\rm coh}}$, obtained by integrating the spectrum over the vortex wavenumbers $m(t) \lesssim k \lesssim f(t)$). The wavenumber $f(t)$ marks the transition scale from vortices to filaments, and $d(t)$ is the leading edge of the 'enstrophy front', assumed to be increasing exponentially. The final coefficient $c(t)$ is proportional to the vortex density. For simplicity we ignore the steep k^4 range expected for $k \ll m$ (Tran & Dritschel, 2006a); this range contributes negligibly to both the energy and the enstrophy. Moreover, we do not incorporate the k^0 range of the equipartition spectrum (A 14), since the transition from k^2 to k^0 in (A 14) occurs at the energy-enstrophy centroid $\sqrt{Q/E} \approx p$, which is much larger than its coherent counterpart $\sqrt{Q_{\rm coh}/E_{\rm coh}}$.

Now vortex self-similarity predicts $c(t) \sim t^{-3/4}$ and $m(t) \sim t^{-3/20}$, but does not predict the 'filament transition' wavenumber $f(t)$. Instead $f(t)$ is determined from conservation of energy E and enstrophy Q, together with the assumption that the growth of the 'enstrophy front' at $k = d(t)$ is exponential, i.e. $d(t) \sim e^{\gamma t}$ where γ is the mean strain rate associated with larger scales. We assume γ scales with the characteristic potential vorticity magnitude q_v, and therefore that γ is constant.

Then, regardless of the transition between the steep intermediate-scale 'vortex spectrum' ck^{-6} and the shallow filamentary spectrum k^{-3} around $k = f$, continuity requires $\mathcal{E}(k,t) \approx cf^{-3}k^{-3}$ in the spectral tail. Now to ensure that the enstrophy in the expanding spectral tail remains finite (and bounded by Q), we must have

$$cf^{-3}\log(d/f) \approx Q \tag{A 16}$$

at late times — when the tail contains essentially all the enstrophy. Now assuming $d \sim e^{\gamma t}$ and using $c(t) \sim t^{-3/4}$ from vortex self-similarity, we obtain the following scaling for the

filament transition wavenumber:

$$f \sim t^{1/12}\,. \tag{A 17}$$

This is a very slow expansion, much slower than found in 2D, cf. (3.6).

This simple model predicts energy growth $\mathcal{E}(k,t) \propto t^{9/20}k^2$ in the equipartition range at large scales $k \ll t^{-3/20}$, energy decay $\mathcal{E}(k,t) \propto t^{-3/4}k^{-6}$ over the vortex population at intermediate scales $t^{-3/20} \ll k \ll t^{1/12}$, and also energy decay $\mathcal{E}(k,t) \propto t^{-1}k^{-3}$ over the filamentary range at small scales $k \gg t^{1/12}$. At late times, essentially all of the energy is contained in scales $k < f$, while all the enstrophy is contained in scales $k > f$.

Appendix B. CASL numerics

Few numerical methods are suited to study a perfectly inviscid fluid. One approach is to use point vortices, as we did in §2 with the vortex-in-cell (VIC) method (cf. Christiansen & Zabusky, 1973). This method is not accurate at scales below the grid (or cell) size, since there vortex interactions are not properly accounted for. As such, its ability to follow the inevitable development of fine-scale structure is very limited. Another approach is to use the Contour-Advective Semi-Lagrangian (CASL) method (Dritschel & Ambaum, 1997), which represents vorticity (or potential vorticity in the 3D QG context) as contours. These contours correspond to jumps in (potential) vorticity, and are material curves in the inviscid dynamics. By using a modest number of contours, one can accurately represent the dynamics of a smoothly-varying vorticity field (cf. Dritschel, Polvani & Mohebalhojeh, 1999 & refs.).

The CASL method, like the VIC method, makes use of an underlying grid, called the 'inversion grid' to compute the velocity field from the vorticity field. The latter is obtained from the contours after a 'contour-to-grid' conversion, but first on a finer grid 4 times finer (in both x and y) than the inversion grid. This finer grid vorticity is then repeatedly 1-2-1 averaged in each spatial direction to obtain the vorticity on the inversion grid. From there, standard FFTs are used to compute the gridded velocity, as in the VIC method. Likewise, the velocity at the points or 'nodes' representing each contour are found by bi-linear interpolation of the gridded velocity field. These points are then moved forward in time using a 4^{th}-order Runge-Kutta time-stepping scheme.

Every few time steps (here 3), the contours are regularised by a process called 'contour surgery' (Dritschel, 1988). Surgery topologically reconnects parts of the same contour or parts of two contours sharing the same vorticity level if the distance between them is less than a certain scale δ called the 'surgical scale'. In the simulation reported, we have chosen $\delta = \Delta x/20$, i.e. a twentieth of the inversion grid scale ($\Delta x/20 \le \delta \le \Delta x/10$ is standard). The small scale of surgery permits one to retain vorticity structure well below the grid scale, and because this subgrid vorticity contributes only weakly to the overall velocity field, a significant portion of this structure is reliable (cf. Dritschel *et al.* 1999 & references therein).

So far, this is standard. What is novel in this context is we have taken extra steps to minimise the total dissipation contributed by surgery. In some test simulations using the original CASL method, we noticed that the effect of surgery (after many applications of it) is to reduce the slope of the *large-scale* end of the spectrum, i.e. it leads to an unphysical energy growth at large scales. It might seem odd that removing structure at a twentieth of the grid scale can do this, but the spectral support of a filament is in fact k^{-1} at large scales, albeit with a very small amplitude. But heavy use of surgery, as in turbulence, can build up this large-scale error.

The cure, we found, is to modify surgery so that it only dissipates in wavenumbers

$k_x, k_y > k_{\max}$, where $k_{\max}$ is the truncation wavenumber (i.e. half the number of grid points used in x and in y). Here, we used a 512×512 grid, so $k_{\max} = 256$. This modification *always* reduces the dissipation due to surgery, since in the wavenumbers $k_x, k_y > k_{\max}$ the dissipation is the same as before, while in the wavenumbers $k_x, k_y \leq k_{\max}$ it is zero.

In order to remove the original surgical error in the wavenumbers $k_x, k_y \leq k_{\max}$, the gridded vorticity fields immediately before and after surgery are compared. The difference is the surgical error in these wavenumbers. This difference is then added to a residual vorticity field ω', which is evolved in spectral space using a standard pseudo-spectral method (details of which may be found in Dritschel *et al.* 1999). At any time, the sum of ω' and the vorticity associated with the contours then gives the total vorticity ω.

The residual vorticity ω' evolves according to

$$\frac{\partial\omega'}{\partial t} + \boldsymbol{u}\cdot\nabla\omega' = \nu_e\Delta\omega' \,, \tag{B 1}$$

with ordinary molecular-like diffusion to prevent the build-up of the ω' at high wavenumbers (in fact, this is the *only* dissipation in the entire method — see below). Numerically, following common practice, the spectrally-transformed version of this equation is solved using an integrating factor to exactly account for the diffusion term. Numerical stability requires $|\boldsymbol{u}|_{\max}\Delta t/\Delta x < 1$, and this is satisfied in the simulation reported by our choice of time step, which is chosen for accurate contour advection: $\Delta t \approx 0.1\pi/\omega_{\max}$ (see Dritschel & Ambaum, 1997). The diffusion coefficient ν_e was chosen by trial and error to be as small as possible without leading to an unphysical upturn of the energy spectrum at high wavenumbers. We took $\nu_e = \omega_{\rm rms}/k_{\max}^2$, where $\omega_{\rm rms} = \sqrt{2Q}$ at the beginning of each simulation period.

The entire simulation was broken up into periods of equal length, here $2T_{\rm eddy}$, where $T_{\rm eddy} \equiv 2\pi/\omega_{\rm rms}(0)$ is defined to be the eddy turnaround time (based on the r.m.s. vorticity at $t = 0$). After every period, various diagnostics were computed, such as spectra and high-resolution images of the vorticity field, and the diffusion coefficient ν_e was reset. Every three periods, the residual vorticity ω' and the vorticity associated with the contours were combined on an ultra-fine grid, 8 times finer in each dimension than the inversion grid. Then, new contours were re-built from this gridded field (using a fast contouring algorithm described in Dritschel & Ambaum, 2006) for use in the next three simulation periods.

Since the gridded vorticity associated with these new contours does not exactly equal the original gridded vorticity before contouring, the difference is used as the initial conditions for ω'. This procedure ensures that there is no change in the total gridded vorticity field as a result of recontouring. Nor is there any change associated with surgery during a simulation. Dissipation occurs *only* through the diffusion of the residual vorticity in (B 1).

The recontouring controls, like surgery, the build up of contour complexity. It further controls any contour crossing errors arising from the re-distribution of nodes on contours (Schaerf, 2006). (Node redistribution takes place after surgery, every 3 time steps.) Recontouring is expensive, however, and cannot be done frequently. But it is required only after significant advection has taken place, i.e. the time it takes for a scale to cascade from the domain scale to the surgical scale, which is always several times $T_{\rm eddy}$. At this frequency, the cost of recontouring is only a few percent of the total simulation cost.

The set of simulations reported in this paper was carried out in a standard $2\pi \times 2\pi$ periodic domain, using a 512×512 inversion grid ($k_{\max} = 256$). Many other simulations were carried out, and the present set was chosen to ensure adequate resolution of the large scales while accurately resolving intermediate to small scales. Initially, we

prescribed a random-phased vorticity field with energy spectrum $\mathcal{E} = Ck^3 \exp[-2k^2/k_0^2]$, with $k_0 = 32$. The constant C was chosen so that the total energy $E = 1/2$ initially (it follows from the form of the spectrum that the total enstrophy $Q = k_0^2 E$). This gridded field was then interpolated to a grid 8 times finer in each dimension to create the initial vorticity contours. Then, the gridded field associated with the contours was found, and the difference from the original vorticity field was used as the initial conditions for the residual field ω'. For example, in one simulation initially, $|\omega|_{\max} = 142.7$ and $|\omega|_{\rm rms} = 31.40$. From this, the time step was chosen to be $\Delta t = 0.00225 \approx 0.1\pi/\omega_{\max} \approx 0.00573 T_{\rm eddy}$, where $T_{\rm eddy} = 0.3926$. For contouring, the vorticity contour interval was chosen to be $\Delta\omega = 5.709$, yielding approximately 50 contour levels overall. Choosing a smaller contour interval means that the residue ω' is smaller, leading to less dissipation, but this comes at a price of carrying (and memory storage of) a larger number of contours. The current choice is a compromise between accuracy and cost. Finally, for contour resolution, we used a typical large-scale length of $L_c = 2\pi/k_0 \approx 0.1963$ and a dimensionless node separation of $\mu = 0.1118$. The latter ensures that the surgical scale $\delta = \Delta x/20$ since $\delta \equiv \mu^2 L_c/4$ (see Dritschel & Ambaum (1997) for details).

GAG is partly supported by the Australian Research Council grant DP0452147. We wish to thank colleagues and staff at the Isaac Newton Institute (Cambridge) for their feedback and support during the 2008 programme on High Reynolds Number Turbulence.

REFERENCES

Batchelor, G. K. 1969 Computation of the energy spectrum in homogeneous two-dimensional turbulence. *Phys. Fluids* **12**, 233–239.

Benzi, R., Patarnello, S. & Santangelo, P., 1988 Self-similar coherent structures in two-dimensional decaying turbulence. *J. Phys. A* **21**, 1221-1237.

Benzi, R., Colella, M., Briscolini, M. & Santangelo, P., 1992 A simple point vortex model for two-dimensional decaying turbulence. *Phys. Fluids* **4**, 1036.

Bracco, A., McWilliams, J. C., Murante, G., Provenzale, A. & Weiss, J. B. 2000 Revisiting freely decaying two-dimensional turbulence at millennial resolution. *Phys. Fluids* **12**, 2931-2941.

Carnevale, G. F, McWilliams, J. C., Pomeau, Y., Weiss, J. B. & Young, W. R., 1991 Evolution of vortex statistics in two-dimensional turbulence. *Phys. Rev. Lett.* **66**, 2735-2737.

Charney, J. 1971 Geostrophic turbulence. *J. Atmos. Sci.* **28**, 1087–1095.

Christiansen, J. P. & Zabusky, N. J. 1973 Instability, coalescence and fission of finite-area vortex structures. *J. Fluid Mech.* **61**, 219–243.

Clercx, H. J. H., Maassen, S. R. & van Heijst, G. J. F. 1999 Decaying two-dimensional turbulence in square containers with no-slip or stress-free boundaries. *Phys. Fluids* **11**, 611-626.

Davidson, P. A. 2004 *Turbulence: An Introduction for Scientists and Engineers.* Oxford Univ. Press, 678pp.

Davidson, P. A. 2007 On the large-scale structure of homogeneous, two-dimensional turbulence. *J. Fluid Mech.* **580**, 431–450.

Dritschel, D. G. 1988 Contour surgery: a topological reconnection scheme for extended integrations using contour dynamics. *J. Comput. Phys.* **77**, 240–266.

Dritschel, D. G. & Waugh, D. W. 1992 Quantification of the inelastic interaction of unequal vortices in two-dimensional vortex dynamics. *Phys. Fluids A* **4**, 1737–1744.

Dritschel, D. G. & Zabusky, N. J. 1996 On the nature of vortex interactions and models in unforced nearly-inviscid two-dimensional turbulence. *Phys. Fluids* **8(5)**, 1252–1256.

Dritschel, D. G. & Ambaum, M. H. P. 1997 A contour-advective semi-Lagrangian algorithm for the simulation of fine-scale conservative fields. *Quart. J. Roy. Meteorol. Soc.* **123**, 1097–1130.

Dritschel, D. G., Polvani, L. M. & Mohebalhojeh, A. R. 1999 The contour-advective semi-Lagrangian algorithm for the shallow water equations. *Mon. Wea. Rev.* **127(7)**, 1551–1565.

Dritschel, D. G. & Ambaum, M. H. P. 2006 The diabatic contour advective semi-Lagrangian algorithm. *Mon. Wea. Rev.* **134(9)**, 2503–2514.

Dritschel, D. G., Tran, C. V. & Scott, R. K. 2007 Revisiting Batchelor's theory of two-dimensional turbulence. *J. Fluid Mech.* **591**, 379–391.

Dritschel, D. G., Scott, R. K., Macaskill, C., Gottwald, G. A. & Tran, C. V. 2008 Unifying scaling theory for vortex dynamics in two-dimensional turbulence. *Phys. Rev. Lett.* **101**, 094501.

Fox, D. G. & Orszag, S. A. 1973 Inviscid dynamics of two-dimensional turbulence. *Phys. Fluids* **16(2)**, 169–171.

Gilbert, A. 1988 Spiral structures and spectra in two-dimensional turbulence. *J. Fluid Mech.* **193**, 475–497.

Gill, A. E. 1982 *Atmosphere-Ocean Dynamics*. Academic

Kraichnan, R. H. 1967 Inertial ranges in two-dimensional turbulence. *Phys. Fluids* **10**, 1417–1423.

McWilliams, J. C, 1984 The emergence of isolated coherent vortices in turbulent flow. *J. Fluid Mech.* **146**, 21-43.

Onsager, L. 1949 Statistical hydrodynamics. *Nuovo Cimento* **6**, 279–287.

Reinaud, J. N., Dritschel, D. G. & Koudella, C. R. 2003 The shape of vortices in quasi-geostrophic turbulence. *J. Fluid Mech.* **474**, 175–192.

Saffman, P. G. 1971 On the spectrum and decay of random two-dimensional vorticity distributions at large Reynolds-number. *Stud. Appl. Math.* **50**, 377–383.

Schaerf, T. 2006 Ph.D. Thesis. *University of Sydney*, On contour crossings in contour-advective simulations of geophysical fluid flows, 197 pp.

Tran, C. V. & Dritschel, D. G. 2006a Large-scale dynamics in two-dimensional Euler and surface quasigeostrophic flows. *Phys. Fluids* **18**, 121703.

Tran, C. V. & Dritschel, D. G. 2006b Vanishing enstrophy dissipation in two-dimensional Navier–Stokes turbulence in the inviscid limit. *J. Fluid Mech.* **559**, 107–116.

Weiss. J. B. & and McWilliams, J. C. 1993 Temporal scaling behavior of decaying two-dimensional turbulence. *Phys. Fluids* **5**, 608-621.